Excited-state odd-even effect in through-space interactions

Zuping Xiong[1,2,3], Jianyu Zhang[4], Jing Zhi Sun[1,3], Haoke Zhang[1,2,3]*, Ben Zhong Tang[1,4,5]*

[1]MOE Key Laboratory of Macromolecular Synthesis and Functionalization, Department of Polymer Science and Engineering, Zhejiang University, Hangzhou 310058, China

[2]Zhejiang-Israel Joint Laboratory of Self-Assembling Functional Materials, ZJU-Hangzhou Global Scientific and Technological Innovation Center, Zhejiang University, Hangzhou 311215, China

[3]Centre of Healthcare Materials, Shaoxing Institute, Zhejiang University, Shaoxing 312000, China

[4]Department of Chemistry, Hong Kong Branch of Chinese National Engineering Research Center for Tissue Restoration and Reconstruction, The Hong Kong University of Science and Technology, Hong Kong, 999077, China

[5]School of Science and Engineering, Shenzhen Institute of Aggregate Science and Technology, The Chinese University of Hong Kong, Shenzhen (CUHK-Shenzhen), Guangzhou 518172, China

Corresponding emails: zhanghaoke@zju.edu.cn (Haoke Zhang); tangbenz@cuhk.edu.cn (Ben Zhong Tang)

Abstract: Odd-even effect is a fantastic phenomenon in nature, which has been applied in diverse fields such as organic self-assembled monolayers and liquid crystals. Currently, the origin of each odd-even effect remains elusive, and all of the reported odd-even effects are about the ground-state properties. Here we discover an excited-state odd-even effect in through-space interaction (TSI) of nonconjugated tetraphenylalkanes (TPAs). The TPAs with an even number of alkyl carbon atoms (**C2-TPA**, **C4-TPA**, and **C6-TPA**) show strong TSI, long-wavelength emission, and high QY. However, the odd ones (**C1-TPA**, **C3-TPA**, **C5-TPA**, and **C7-TPA**) are almost nonemissive with negligible QY. Systematically experimental and theoretical results reveal that the excited-state odd-even effect is synthetically determined by three factors: alkyl geometry, molecular moveability, and intermolecular packing. Moreover, these flexible luminescent TPAs possess tremendous advantages in fluorescent information encryptions. This work extends the odd-even effect to photophysics, demonstrating its substantial importance and universality in nature.

Wondrous odd-even effects are widely observed in nature, including biology, social behaviors, mathematics, and so forth. Additionally, modern materials science also fully exploits the odd-even effect to design excellent artificial materials[1-7]. As shown in Fig. 1, the different orientations of the terminal methyl groups in self-assembled *n*-alkanethiolate monolayers on Au (111) induce odd-even alterations of macroscopic properties[8]. Moreover, carbon chains with an odd or even number of methine groups could even lead to molecules with different helicity[9]. Therefore, it is evident that this captivating effect possesses significant technological potential.

Excited states play a crucial role in many natural processes, such as biological evolution and material creation, particularly in the case of photophysical processes. It is still a virgin land to manipulate photophysical processes through the odd-even effect. One of the difficulties in regulating the excited-state properties is the short lifetime and rigid conformation of most traditional luminophores[10,11]. Such rigid planar structures always exhibit small conformational changes from ground to excited state, resulting in the undiscovered excited-state odd-even effect (ESODE). Recently, there has been a new class of propeller-shaped luminescent molecules with aggregation-induced emission (AIE) behaviors, which usually have a large Stokes shift due to the significant excited-state conformational change[12-15]. Besides, compared with the conventional planar π-conjugated luminophores, the emission of twisted AIE luminophores could be attributed to the effective through-space interaction (TSI) among different subunits[16]. Scientists have discovered some special nonconjugated AIE luminophores which have more flexible conformation and stronger TSI than conjugated sysytems[17-23]. Thus, this intrinsic feature of nonconjugated luminophores may offer the possibility for manipulating the excited-state processes by the odd-even effect.

Herein we design a series of nonconjugated tetraphenylalkanes (TPAs) with different lengths of alkyl chains from methane to heptane, as shown in Fig.1. In these TPAs, the bilateral diphenylmethyl (DPM) parts can be regarded as subunits, which is bridged by the middle alkyl chains whose carbon atoms gradually increases from one carbon (**C1-TPA**) to seven carbons (**C7-TPA**). It is found that these TPAs show a typical ESODE. The TPAs with an even number of alkyl carbons show strong TSI, long-wavelength emission, and high QY. However, the odd ones are almost nonemissive with negligible QY. Further investigations demonstrated that the ESODE is synthetically determined by three factors: alkyl geometry, molecular moveability, and intermolecular packing. Finally, these luminescent TPAs were successfully used for fluorescent information encryptions by virtue of their flexible conformation.

Results and discussion

Photophysical performances

Tetraphenylalkanes with different chain lengths (from one to seven) were prepared (Supplementary Fig. 1) and fully characterized (Supplementary Figs. 2-32). Their nonconjugated electronic structures are confirmed by the absorption and photoluminescence (PL) spectra in the isolated state (Supplementary Figs. 33-34). The aggregates of these compounds were gradually formed when

different volume fractions of water were added to their acetonitrile (ACN) solution. The PL characterization suggests that the TSI strength of these aggregates follows the order of **C2-TPA** > **C1-TPA** > **C3-TPA** > **C4-TPA** > **C5-TPA** > **C6-TPA** > **C7-TPA**, which is read from the intensity of long-wavelength emission corresponding to the TSI (Supplementary Fig. 35). According to our previous results, such order of the TSI should closely relate to structural flexibility (ability to form TSI) and rigidity (ability to stabilize TSI)[24,25]. Generally, the mixed solvent of ACN/water will affect the photophysical properties of the aggregates in the solution. To reveal their accurate electronic structures in the aggregate state, their photophysical properties in the crystalline state were explored. Figs. 2a-g exhibit the PL spectra of these TPAs in the crystalline state with different excitation wavelengths (λ_{ex}) from 240 to 360 nm. In Fig. 2a, **C1-TPA** crystal only shows a weak peak with a maximum emission wavelength (λ_{em}) at 383 nm, suggesting that the excessively rigid structure is not conducive to forming strong TSI. However, from **C1-TPA** to **C2-TPA**, decreasing the intramolecular steric hindrance induces better luminescence properties. As shown in Fig. 2b, **C2-TPA** exhibits a strong and redshifted emission peak at 463 nm. Meanwhile, the PL peak is excitation-independent within the λ_{em} from 240 to 360 nm. When the chain length of the middle alkyl is increased to three, TSI is almost absent in **C3-TPA** which only has the intrinsic emission from isolated benzene rings with λ_{em} of 290 nm (Fig. 2c). Surprisingly, further increasing the chain length does not weaken the PL performance. In contrast, **C4-TPA** even shows two kinds of strong TSIs with two emission peaks observed at 311 nm and 432 nm, respectively (Fig. 2d). According to our previous results, the PL peak at 311 nm was ascribed to the homoconjugation of diphenylmethane moieties and the long-wavelength emission at 432 nm should arise from the secondary TSI among four phenyl rings[26]. These results also suggest that the TSI in TPAs is not exclusively affected by structural flexibility and rigidity, as other factors appear to play a dominant role in determining their PL properties. Furthermore, **C5-TPA** only exhibits weak TSI as reflected by its blueshifted emission (λ_{em} = 350 nm), while the strong and long-wavelength emission at 446 nm reappeared in **C6-TPA** (Fig. 2e and 2f). However, when the alkyl chain length increases to seven, the photophysical properties become different, and **C7-TPA** crystal displays the excitation-depended emission. As shown in Fig. 2g, the λ_{em} increases from 373 to 435 nm when the λ_{ex} shifts from 240 to 360 nm, demonstrating that **C7-TPA** has unstable and weak TSI.

The λ_{em} of these seven compounds under λ_{ex} of 300 nm was summarized in Fig. 2h. It shows an obvious ESODE that the even number of alkyl chain lengths (**C2-TPA**, **C4-TPA**, and **C6-TPA**) has longer λ_{em} and stronger TSI than the odd ones (**C1-TPA**, **C3-TPA**, **C5-TPA**, and **C7-TPA**). This ESODE is also confirmed by their solid-state fluorescence quantum yields (QYs) (Fig. 2i). The QYs of **C2-TPA**, **C4-TPA**, and **C6-TPA** are 68%, 45%, and 43%, respectively, but **C1-TPA**, **C3-TPA**, and **C7-TPA** are only around 5%. Moreover, their radiative decay rate constants (k_r) calculated by the solid-state lifetime and QYs also follow the odd-even effect (Supplementary Figs. 36-37). However, what is the underlying mechanism of ESODE in TSI?

Theoretical calculation on conformations and electronic structures

To reveal the nature of ESODE in TSI, the natural transition orbitals (NTOs)[27] of all TPAs were calculated and plotted in Fig. 3a. For **C1-TPA**, it seems that the TSI occurs between two adjacent phenyl rings but not among all four phenyl rings. From **C2-TPA** to **C5-TPA**, a significant TSI was observed between two phenyl rings from different DPM subunits, generating secondary TSI. However, when the alkyl chain length is further increased, the two DPM subunits in **C6-TPA** and **C7-TPA** could not approach each other closely to form an effective TSI, and only the homoconjugation of DPM is observed. Mapping the frontier molecular orbitals (FMOs) also verified the above results (Supplementary Fig. 38). Since all these seven compounds show TSI in the excited state, it suggests that the static conformations could not be used to disclose their PL properties. Thus, the dynamic change of conformation was then investigated from ground to excited states. As shown in Fig. 3b and Supplementary Fig. 39, the distance ($d_{C\text{-}C}$) of two sp^2 carbon atoms located on different DPM subunits and linked to the sp^3 carbon was analyzed for all the TPAs. At ground state, the d_{S0} increases from 2.469 Å (**C1-TPA**) to 9.445 Å (**C7-TPA**). Meanwhile, the excited-state distance (d_{S1}) also increases from 2.396 Å (**C1-TPA**) to 9.466 Å (**C7-TPA**). It is noteworthy that the $d_{C\text{-}C}$ is shortened for **C1-TPA** to **C5-TPA** from the ground to the excited state, showing a negative $d_{(S1\text{-}S0)}$. Moreover, the shortening magnitude keeps increasing from **C1-TPA** (-0.073 Å) to **C5-TPA** (-1.041 Å). However, **C6-TPA** and **C7-TPA** show positive $d_{(S1\text{-}S0)}$, exhibiting an elongation of the alkyl chain.

Fig. 3c vividly illustrates the above results about the light-driven intramolecular motion. After the photoexcitation, **C1-TPA** to **C5-TPA** show a shortened length of the alkyl chain and the two DPM subunits approach each other, but the alkyl chain is elongated in **C6-TPA** and **C7-TPA**. Besides, the single-molecule movability of these TPAs was investigated by using the parameter of root-mean-square deviation (RMSD), which indicated the structural variation from ground to excited state. As shown in Fig. 3d, the value of RMSD increased from **C1-TPA** (0.054 Å) to **C5-TPA** (0.721 Å), suggesting that the molecular flexibility increased with the increasing length of the alkyl chain. Whereas, when the chain length is further increased, the conformation of **C6-TPA** and **C7-TPA** becomes rigid with RMSD values of 0.383 and 0.342 Å, respectively. Based on the above analysis of static TSI and dynamic conformation, these seven TPAs could be divided into two groups, i) **C1-TPA** to **C5-TPA** with shortening alkyl chain after photoexcitation and increasing structural flexibility; ii) **C6-TPA** and **C7-TPA** with lengthening alkyl chain after photoexcitation and decreasing structural flexibility.

Mechanistic pictures of the excited-state odd-even effect

To construct a clear relationship between the conformation and PL properties, the optimized ground- and excited-state conformations were carefully analyzed. As **C1-TPA** to **C5-TPA** showed different structural properties with **C6-TPA** and **C7-TPA**, they were investigated separately. Fig. 4a-d shows that **C2-TPA** and **C4-TPA** with an even number of alkyl carbons exhibit staggered intramolecular packing structures in which the two vicinal phenyl rings are close to each other but do not form a

face-to-face geometry. On the contrary, **C3-TPA** and **C5-TPA** with an odd number of alkyl carbons show a face-to-face conformation. These two structures could be quantificationally represented by the percentage of the overlapping area (POA). The larger of POA, the more overlapped vicinal phenyl rings. The calculated POA is 0%, 100%, 5.4%, and 82% for **C2-TPA**, **C3-TPA**, **C4-TPA**, and **C5-TPA**, respectively, confirming these two kinds of TSI: staggered TSI (**C2-TPA** and **C4-TPA**) and face-to-face TSI (**C3-TPA** and **C5-TPA**) (Supplementary Fig. 40). Considering their PL behaviors, it suggests that the staggered TSI with a small POA corresponding to even TPAs shows high PL efficiency (bright state). On the contrary, the face-to-face TSI with a large POA corresponding to odd TPAs is nonemissive (dark state) (Fig. 4e). Such kind of intramolecular face-to-face TSI is quite similar to the well-studied intermolecular H-aggregate which is always nonemissive[28,29]. Once again, these results prove the important role of molecular packing in the photophysical properties. Since the different kinds of TSI (staggered and face-to-face) were revealed to induce the ESODE, why the different lengths of the alkyl chain can regularly generate these two kinds of intramolecular packing? After carefully analyzing the structures, we discovered that the arrangement of these two vicinal phenyl rings depended on the orientation of the terminal methyl groups. For **C3-TPA** and **C5-TPA**, these two terminal methyl groups are located on the same side, generating the close and face-to-face packing of two vicinal phenyl rings. However, for **C2-TPA** and **C4-TPA** with an even number of alkyl carbons, its two terminal methyl groups are located on different sides, then the associated two vicinal phenyl rings are relatively far away from each other and form the staggered TSI. It is noteworthy that **C1-TPA** also has staggered TSI because of its larger intramolecular steric hindrance than the other TPAs with longer alkyl chains, but the rigid conformation weakens the strength of its staggered TSI as discussed above. These results demonstrate that the ESODE of **C1-TPA** to **C5-TPA** synergistically stems from the geometry of the alkyl chain and the molecular moveability.

However, what happens for the second-group compounds (**C6-TPA** and **C7-TPA**)? Fortunately, we obtained the single crystal structure of **C6-TPA** and discovered the presence of two intermolecular benzene rings close to each other. The crystal packing and Hirshfeld surfaces analysis demonstrate that there is almost no intermolecular TSI for the first-group compounds (Supplementary Fig. 41). However, two **C6-TPA** molecules have strong intermolecular π-π interaction reflected by the short C-C distance of around 3.4 Å (Fig. 5a). Meanwhile, theoretical calculations based on the selected dimer from crystal structure show significant intermolecular orbital overlaps between two intermolecular DPM subunits. Then intrafragment charge transfer (IFCT) based on the optimized first excited state (crystalline phase) quantitatively proves the presence of intermolecular staggered TSI, which corresponds to red columns (Fig. 5b, right). Besides the significant intramolecular electron transfer between Ph-2 and Ph-3 (0.317), the intermolecular charge transfer is diverse with the sum of 0.279, resulting in the efficient emission of **C6-TPA**. Similar to **C3-TPA** and **C5-TPA**, it is also too difficult to get a suitable single crystal of **C7-TPA** for X-ray diffraction (XRD) characterization, suggesting that alkyl chains containing an odd number of carbon atoms do not promote orderly intermolecular stacking. It also implies that

consistent orientations of the terminal DPM at the end of the same alkyl chain may hinder molecules from approaching each other closely. As a result, the ESODE in **C6-TPA** and **C7-TPA** could be attributed to their different intermolecular TSI rather than intramolecular interaction. To further prove the different emission sources (intramolecular or intermolecular TSI) of these two kinds of TPAs, temperature-dependent PL spectra were recorded for the crystals of **C2-TPA**, **C4-TPA**, and **C6-TPA**. As shown in Fig. 5c, the PL intensity of **C2-TPA** decreases with the increased temperature from 77 to 297 K, especially above 237 K. Meanwhile, a significant redshift of λ_{em} (450 to 470 nm) is associated. **C4-TPA** exhibits a similarly sharp and continuous decrease in PL intensity along with the increased temperature (Fig. 5d). These results suggest that the intramolecular TSI is weakened when the temperature increases, which should be ascribed to the intensified intramolecular motions at high temperatures, resulting in unstable TSI. However, the change of PL intensity for **C6-TPA** crystal is divided into two stages (I: 77 to 177 K; II: 177 to 297 K) (Fig. 5e). In the first stage, the **C6-TPA** crystal shows an obvious fluorescence enhancement when the temperature increases from 77 to 177 K. When the temperature is further increased to 297 K, the PL intensity is gradually weakened. The decrease of PL intensity in the second state should have a similar mechanism to the behavior of **C2-TPA** and **C4-TPA**. However, the enhanced PL intensity in the first stage suggests that increasing temperature should be conducive to forming intermolecular TSI. In other words, the light-driven intermolecular TSI could be boosted by vigorous molecular motions[30]. The temperature-dependent PL measurements prove that the blue emission of **C2-TPA** and **C4-TPA** comes from the intramolecular TSI, but intermolecular TSI plays a dominant role in the PL properties of **C6-TPA**. In summary, the overall ESODE for these TPAs is synthetically determined by three factors, involving the alkyl geometry, molecular moveability, and intermolecular packing.

Information encryption

The success of the ESODE in regulating TSI is partly attributed to the exceptional flexibility of these nonconjugated luminogens, which distinguishes them from π-conjugated luminophores. As a result, these nonconjugated flexible luminophores demonstrate more sensitive responsiveness to external stimuli compared to π-conjugated luminophores. For example, alkene-based tetraphene butadiene (TPB) and alkane-based **C4-TPA** both exhibit blue emission in the crystalline state (Fig. 6a), but the bright emission of **C4-TPA** disappears thoroughly once it is dispersed in polymethyl methacrylate (PMMA) film. On the contrary, TPB still shows bright blue emission when it is dispersed in PMMA, and a faint emission is also observed in its acetonitrile solution ($c = 5\times10^{-3}$ M). The above results prove the more sensitive responsiveness of nonconjugated luminogens. Such a conclusion could also be proved by a relaxed scan of the potential energy surface and the calculation of reorganization energies (Supplementary Figs. 42-45). Based on the above properties, two real 3D models of chameleons were printed, and their surfaces were coated with TPB and **C4-TPA**, respectively. As shown in Fig. 6b, these two coated models both show bright blue emission under 365 nm UV light. Then the time-dependent stimulus-responsive process was studied, and these two systems exhibited different changes in emission intensity under the treatment of tetrahydrofuran

(THF) fuming. The results also suggest that **C4-TPA** shows a more sensitive response to fuming than TPB. Accordingly, fluorescent encryptions (two-dimensional code, QR Code) were achieved by using TPB and **C4-TPA** simultaneously. As shown in Fig. 6c, two glasses were coated with TPB film (TPB@PMMA), and partial information about the QR code was loaded. Meanwhile, the central part of the QR code was designed as the key to realizing fluorescent encryption. The top part of this key was coated with TPB and **C4-TPA** solids, and the bottom part was still coated with TPB solids. At this stage, the assembled QR code is invalid without any information. However, the **C4-TPA** parts in the key area are gradually darkened after fuming with THF for 20 minutes. This new QR code exhibits the correct pattern for unlocking, showing effective information. Drying the key (filter paper) could recover the bright blue emission of the **C4-TPA** part. Thus, the QR code could be locked again by natural drying once the correct information is read. The whole process is almost imperceptible under daylight.

Conclusions

The nonconjugated tetraphenylalkanes system reveals a wondrous ESODE in TSI. The TPAs with an even number of alkyl carbons show strong TSI, long-wavelength emission, and high QY. However, the odd ones are almost nonemissive with negligible QY. Experimental characterization and theoretical calculation demonstrate that for the TPAs of **C1-TPA** to **C5-TPA**, the alkyl chain with an even number of carbon atoms leads to the staggered TSI for excellent photoluminescence while that with the odd number of carbon atoms results in the face-to-face TSI for efficient nonradiative decay, which is determined by the synergistic effects: geometry of terminal carbons in the alkyl chain and molecular moveability. Meanwhile, the odd-even effect of **C6-TPA** and **C7-TPA** with long alkyl chains is induced by their different intermolecular TSI rather than intramolecular interaction, as evidenced by **C6-TPA** with a long-range ordered packing with strong intermolecular TSI. Moreover, reliable fluorescent information encryptions are realized based on the flexible nature of these luminescent TPAs which show more sensitive responsiveness than π-conjugated luminophores. This work not only discovers a charming photophysical phenomenon about the excited-state odd-even effect but also reveals the underlying mechanism. It is foreseeable that the odd-even effect about the length of the alkyl chain widely exists in many physical, chemical, and biological properties, which is an essential component of natural laws.

Online content

Any reporting summaries, source data, extended data, supplementary information, acknowledgments, peer review information; details of author contributions and competing interests; and statements of data and code availability are available at https://doi.org/.

Reference

1. Uchida, H., Miyata, K., Oba, M., Ishii, T., Suma, T., Itaka, K., Nishiyama, N., Kataoka, K. Odd–even effect of repeating aminoethylene units in the side chain of n-substituted polyaspartamides on gene transfection profiles. *J. Am. Chem. Soc.* **133**, 15524-15532 (2011).
2. Wang, Z., Chen, J., Martin, A., Raturi, D., Thuo, M. Role of nanoscale roughness and polarity in odd–even effect of self-assembled monolayers. *Angew. Chem. Int. Ed.* **61**, e202205251 (2022).
3. Mishra, M. K., Varughese, S., Ramamurty, U., Desiraju, G. R. Odd–even effect in the elastic modulii of α,ω-alkanedicarboxylic acids. *J. Am. Chem. Soc.* **135**, 8121-8124 (2013).
4. Yang, K., Cai, Z., Jaiswal, A., Tyagi, M., Moore, J., Zhang, Y. Dynamic odd-even effect in liquid n-alkanes near their melting points. *Angew. Chem. Int. Ed.* **55**, 14090-14095 (2016).
5. Jiang, L., Sangeeth, C., Nijhuis, C. The origin of the odd–even effect in the tunneling rates across EGaIn junctions with self-assembled monolayers (sams) of n-alkanethiolates. *J. Am. Chem. Soc.* 137, 10659-10667 (2015).
6. Marty, R., Nigon, R., Leite, D., Frauenrath, H. Two-fold odd–even effect in self-assembled nanowires from oligopeptide-polymer-substituted perylene bisimides. *J. Am. Chem. Soc.* **136**, 3919-3927 (2014).
7. Wang, J., Schrade, C., Levajac, V., Driel, D., Li, K., Gazibegovic, S., Badawy, G., Veld, R., Lee, J., Pendharkar, M., Dempsey, C., Palmstrøm, C., Bakkers, E., Fu, L., Kouwenhoven, L., Shen, J. Supercurrent parity meter in a nanowire Cooper pair transistor. *Sci. Adv*. **8**, eabm9896 (2022).
8. Amara, F., Dionne, E., Kassir, S., Pellerin, C., Badia, A. Molecular origin of the odd–even effect of macroscopic properties of n-alkanethiolate self-assembled monolayers: bulk or interface? *J. Am. Chem. Soc.* **142**, 13051-13061 (2020).
9. Pradeilles, J. A., Zhong, S., Baglyas, M., Tarczay, G., Butts, C., Myers, E., Aggarwal, V. Odd–even alternations in helical propensity of a homologous series of hydrocarbons. *Nat. Chem*. **12**, 475–480 (2020).
10. Saal, F., Zhang, F., Holzapfel, M., Stolte, M., Michail, E., Moos, M., Schmiedel, A., Krause, A.-M., Lambert, C., Würthner, F., Ravat, P., [n]Helicene diimides (n = 5, 6, and 7): through-bond versus through-space conjugation. *J. Am. Chem. Soc.* **142**, 21298-21303 (2020).
11. Hoffmann, R. Interaction of orbitals through space and through bonds. *Acc. Chem. Res*. **4**, 1−9 (1971).
12. Xia, Q., Zhang, Y., Li, Y., Li, Y., Li, Y., Feng, Z., Fan, X., Qian, J., Lin, H., A historical review of aggregation-induced emission from 2001 to 2020: A bibliometric analysis. *Aggregate* **3**, e152 (2022).
13. Sturala, J., Etherington, M. K., Bismillah, A. N., Higginbotham, H. F., Trewby, W., Aguilar, J. A., Bromley, E. H. C., Avestro, A.-J., Monkman, A. P., McGonigal, P. R. Excited-state aromatic interactions in the aggregation-induced emission of molecular rotors. *J. Am. Chem. Soc*. **139**, 17882−17889 (2017).
14. Liu, B., Tang, B. Z. Aggregation-induced emission: more is different. *Angew. Chem. Int. Ed.* 59, 9788-9789 (2020).
15. Niu, G., Zheng, X., Zhao, Z., Zhang, H., Wang, J., He, X., Chen, Y., Shi, X., Ma, C., Kwok, R., Lam, J., Sung, H., Williams, I., Wong, K., Wang, P., Tang, B. Z., Functionalized acrylonitriles with aggregation-induced emission: structure tuning by simple reaction-condition variation, efficient red emission, and two-photon bioimaging. *J. Am. Chem. Soc*. **141**, 15111-15120 (2019).

16. Liu, J., Zhang, H., Hu, L., Wang, J., Lam, J. W. Y., Blancafort, L., Tang, B. Z. Through-Space Interaction of Tetraphenylethylene: What, Where, and How. *J. Am. Chem. Soc.* **144**, 7901–7910 (2022).
17. Zhang, H., Zheng, X., Xie, N., He, Z., Liu, J., Leung, N. L. C., Niu, Y., Huang, X., Wong, K. S., Kwok, R. T. K., Sung, H. H. Y., Williams, I. D., Qin, A., Lam, J. W. Y., Tang, B. Z. Why do simple molecules with "isolated" phenyl rings emit visible light? *J. Am. Chem. Soc*. **139**, 16264−16272 (2017).
18. Zhang, J., Hu, L., Zhang, K., Liu, J., Li, X., Wang, H., Wang, Z., Sung, H. H. Y., Williams, I. D., Zeng, Z., Lam, J. W. Y., Zhang, H., Tang, B. Z. How to manipulate through-space conjugation and clusteroluminescence of simple AIEgens with isolated phenyl rings. *J. Am. Chem. Soc*. **143**, 9565−9574 (2021).
19. Chu, B., Zhang, H., Chen, K., Liu, B., Yu, Q., Zhang, C., Sun, J., Yang, Q., Zhang, X., Tang, B. Z., Aliphatic polyesters with white-light clusteroluminescence. *J. Am. Chem. Soc*. **144**, 15286-15294 (2022).
20. Zhang, Z., Zhang, J., Xiong, Z., Chu, B., Zhang, C., Sun, J. Z., Zhang, H., Zhang, X., Tang, B. Z., NIR clusteroluminescence of non-conjugated phenolic resins enabled by through-space interactions. *Angew. Chem. Int. Ed.*, e202306762 (2023).
21. Crocker, R., Pace, D., Zhang, B., Lyons, D., Bhadbhade, M., Wong, W, Mai, B., Nguyen, T. Unusual alternating crystallization-induced emission enhancement behavior in nonconjugated ω-phenylalkyl tropylium salts. *J. Am. Chem. Soc*. **143**, 20384-20394 (2021).
22. Zhang, H., Zhao, Z., Turley, A. T., Wang, L., McGonigal, P. R., Tu, Y., Li, Y., Wang, Z., Kwok, R. T. K., Lam, J. W. Y., Tang, B. Z., Aggregate science: from structures to properties. *Adv. Mater*. **32**, 2001457 (2020).
23. Zhang, Z., Xiong, Z., Chu, B., Zhang, Z., Xie, Y., Wang, L., Sun, J. Z., Zhang, H., Zhang, X. H., Tang, B. Z., Manipulation of clusteroluminescence in carbonyl-based aliphatic polymers. *Aggregate* **3**, e278 (2022).
24. Chu, B., Zhang, H., Hu, L., Liu, B., Zhang, C., Zhang, X., Tang, B. Z. Altering chain flexibility of aliphatic polyesters for yellow-green clusteroluminescence in 38 % quantum yield. *Angew. Chem. Int. Ed.* **61**, e202114117 (2022).
25. Xiong, Z., Zhang, J., Wang, L., Xie, Y., Wang, Y., Zhao, Z., Zhang, H., Sun, J. Z., Huang, F., Tang, B. Z., Controllable secondary through-space interaction and clusteroluminescence. *CCS Chem.* 1-13 (2023). https://doi.org/10.31635/ccschem.023.202302815.
26. Liu, J., Zhang, H., Hu, L., Wang, J., Lam, J., Blancafort, L., Tang, B. Z. Through-space interaction of tetraphenylethylene: what, where, and how. *J. Am. Chem. Soc*. **144**, 7901–7910 (2022).
27. Martin, R. Natural transition orbitals. *J. Chem. Phys*. **118**, 4775 (2013).
28. Hestand, N. J., Spano, F. C. Expanded theory of H- and J-molecular aggregates: the effects of vibronic coupling and intermolecular charge transfer. *Chem. Rev.* **118**, 7069-7163 (2018).
29. Tang, N., Zhou, J., Wang, L., Stolte, M., Xie, G., Wen, X., Liu, L., Würthner, F., Gierschner, J., Xie, Z. Anomalous deep-red luminescence of perylene black analogues with strong π-π interactions. *Nat. Commun.* **14**, 1922 (2023).
30. Zhang, H.; Du, L., Wang, L., Liu, J., Wan, Q., Kwok, R. T. K., Lam, J. W. Y., Phillips, D. L., Tang, B. Z. Visualization and Manipulation of Molecular Motion in the Solid State through Photoinduced Clusteroluminescence. *J. Phys. Chem. Lett.* **10**, 7077–7085 (2019).

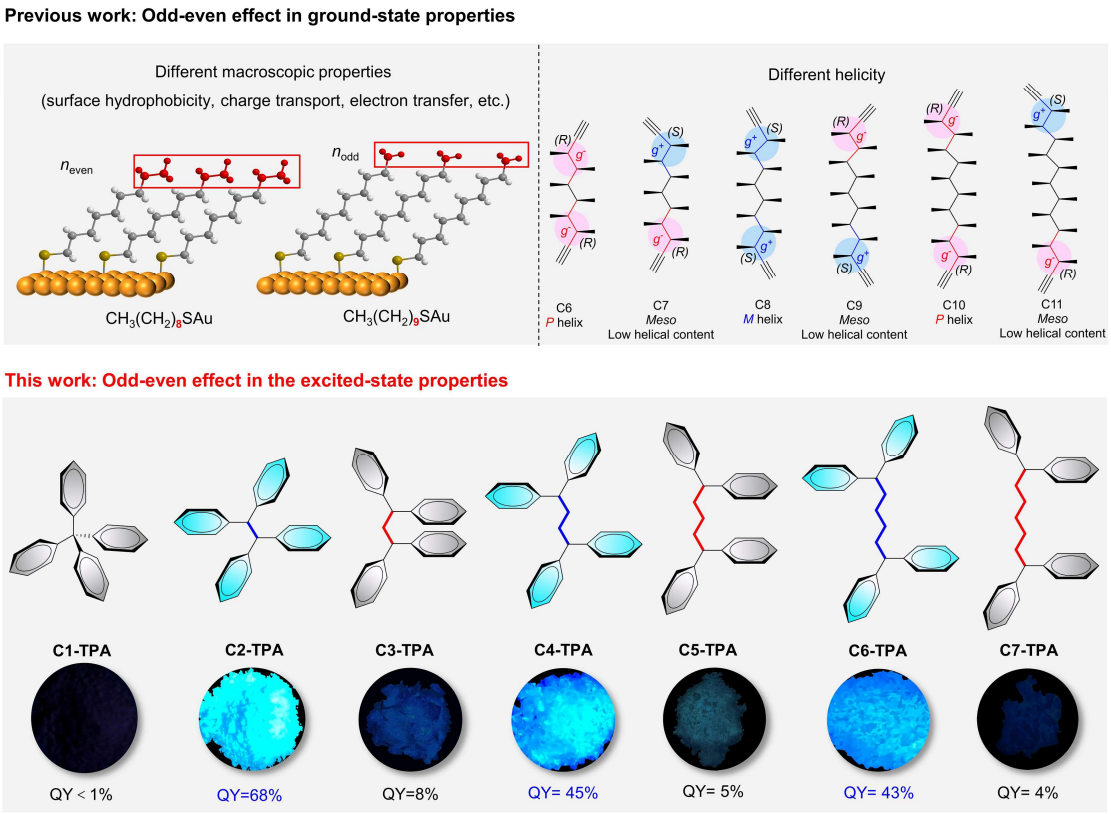

Fig. 1 | Previous works about the odd-even effect in ground-state properties. Upper left: The different macroscopic properties of organic self-assembled monolayers on Au (111) originated from the orientation of the terminal methyl groups depending on whether there is an odd or even number of the alkyl chain. Upper right: Significant odd-even effect in the helical propensity of all-*syn* contiguously methyl-substituted hydrocarbons with chain lengths from C6 to C11. **Odd-even effect in the excited-state properties in this work.** The photophysical properties of nonconjugated tetraphenylalkanes are regulated by the length of alkyl chain.

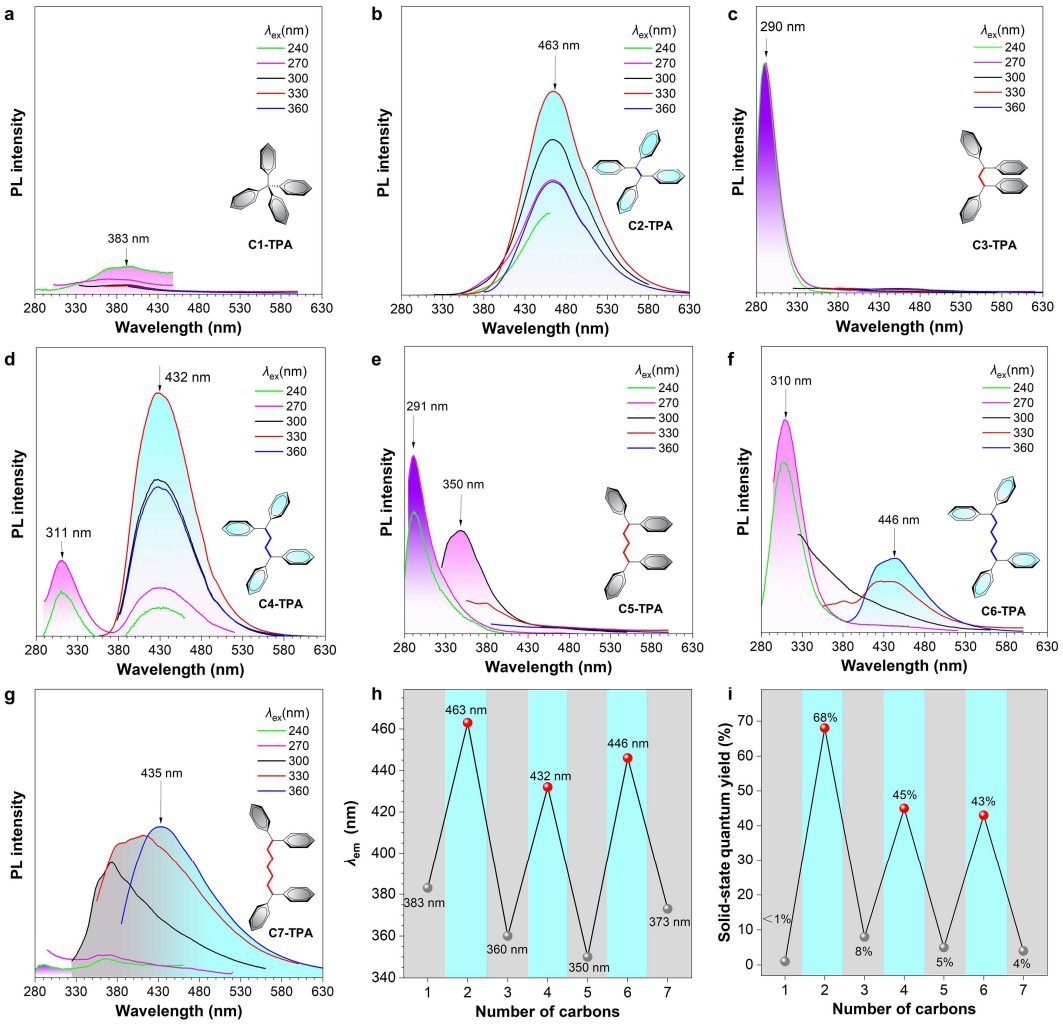

Fig. 2 | Photophysical properties at the crystalline state. PL spectra of a) **C1-TPA**, b) **C2-TPA**, c) **C3-TPA**, d) **C4-TPA**, e) **C5-TPA**, f) **C6-TPA**, and g) **C7-TPA** crystals with different excitation wavelengths (λ_{ex}). h) Plot of maximum emission wavelength (λ_{em}) of their crystals with λ_{ex} = 300 nm. i) Plot of luminescence quantum yield of their crystals with λ_{ex} = 300 nm.

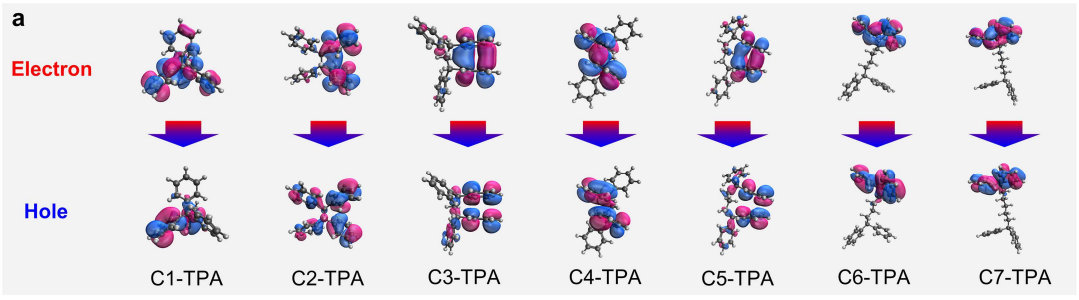

$d_{C\text{-}C}$	C1-TPA	C2-TPA	C3-TPA	C4-TPA	C5-TPA	C6-TPA	C7-TPA
d_{S0} (Å)	2.469	3.072	3.261	4.298	4.941	7.093	9.445
d_{S1} (Å)	2.396	2.927	2.825	3.559	3.900	7.196	9.466
$d_{(S1\text{-}S0)}$ (Å)	**-0.073**	**-0.145**	**-0.436**	**-0.739**	**-1.041**	**0.103**	**0.021**

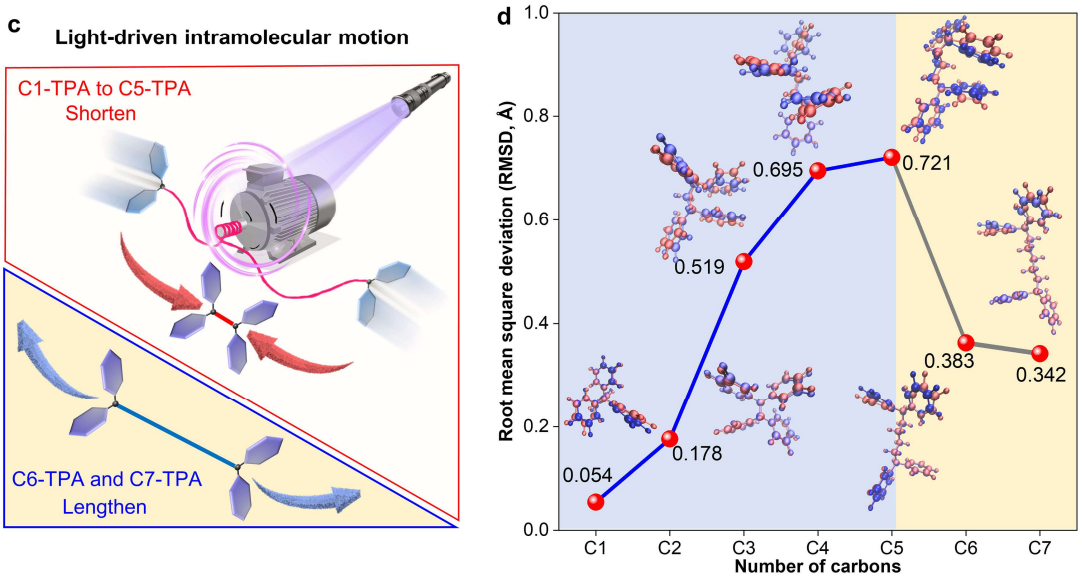

Fig. 3 | Light-driven intramolecular motion of C1-TPA to C7-TPA. a Natural transition orbitals of the optimized excited state at the gas phase. **b** The distance of carbon atoms connected by dotted lines ($d_{C\text{-}C}$) changed from the ground state (d_{S0}) to the excited state (d_{S1}) during the optimization. **c** Schematic illustration of the light-driven intermolecular motion of these tetraphenylalkanes from S_0 to S_1. **d** Plot of root-mean-square deviation (RMSD) versus the different tetraphenylalkanes with various lengths of alkyl chain.

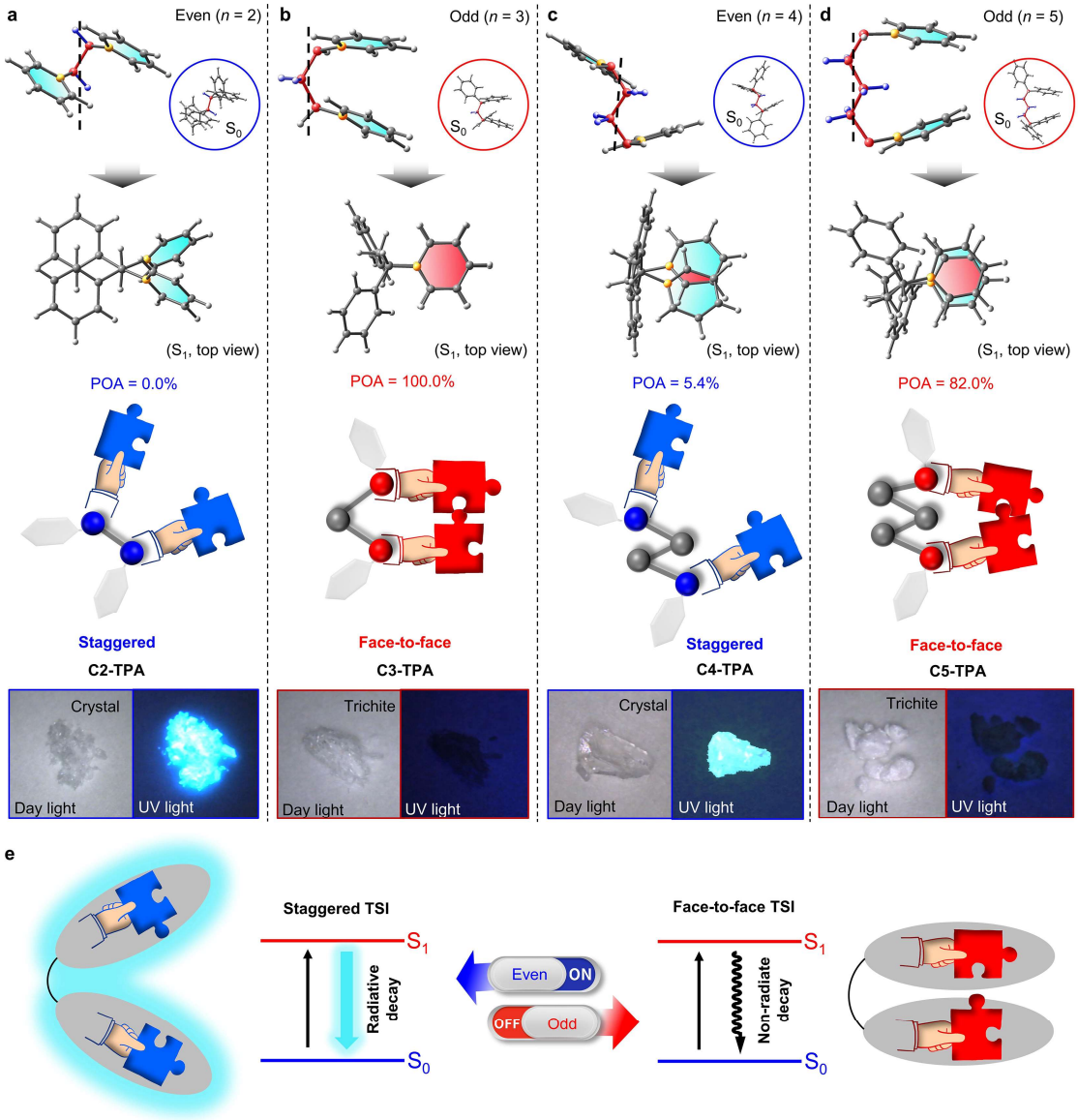

Fig. 4 | The intramolecular staggered or face-to-face packing structures of C1-TPA to C5-TPA. Optimized ground- (S_0) and excited-state (S_1) geometries of **a C2-TPA**, **b C3-TPA**, **c C4-TPA**, and **d C5-TPA** (note: two farthest phenyl rings are hidden to show the orientation of terminal phenyl rings which involved in orbital overlap; percentage of the overlapping area (POA) calculated by the software, ImageJ.). Schematic illustration of distinctly different TSIs manipulated by excited-state odd-even effect. Insets: photographs (daylight) and fluorescence photographs of **C2-TPA** to **C5-TPA** (λ_{ex} = 365 nm). **e** Schematic illustration of the different photophysical processes switched by excited-state odd-even effect.

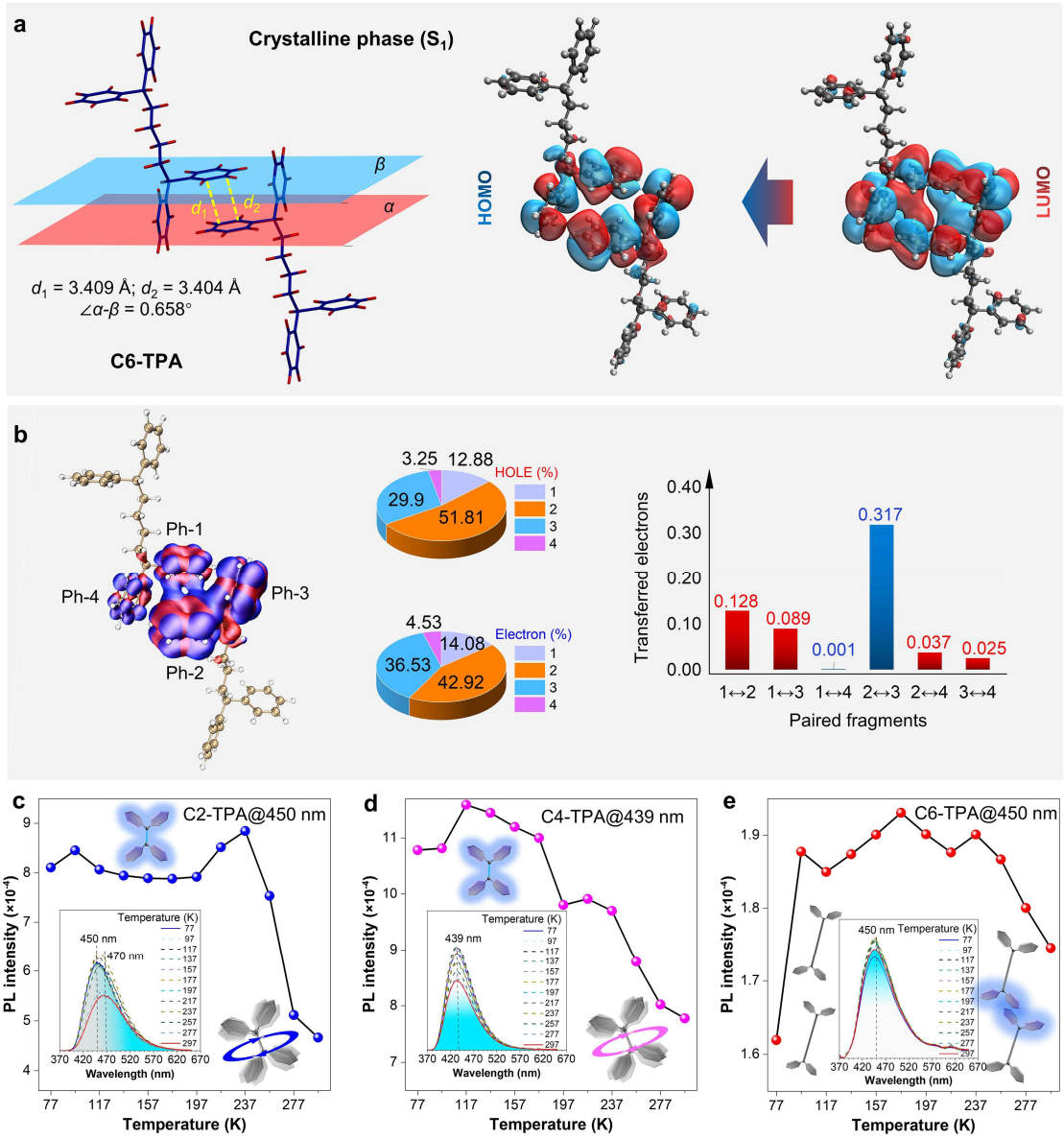

Fig. 5 | Intermolecular through-space interaction analysis. a The intermolecular packing of **C6-TPA** dimer in the excited state (S_1, crystalline phase) and its frontier molecular orbitals. **b** Hole-electron analysis, and transferred electrons of paired fragments for **C6-TPA** dimer (S_1, crystalline phase). **c-e** Temperature-dependent PL of **C2-TPA**, **C4-TPA**, and **C6-TPA** crystals from 77 to 297 K under λ_{ex} of 360 nm.

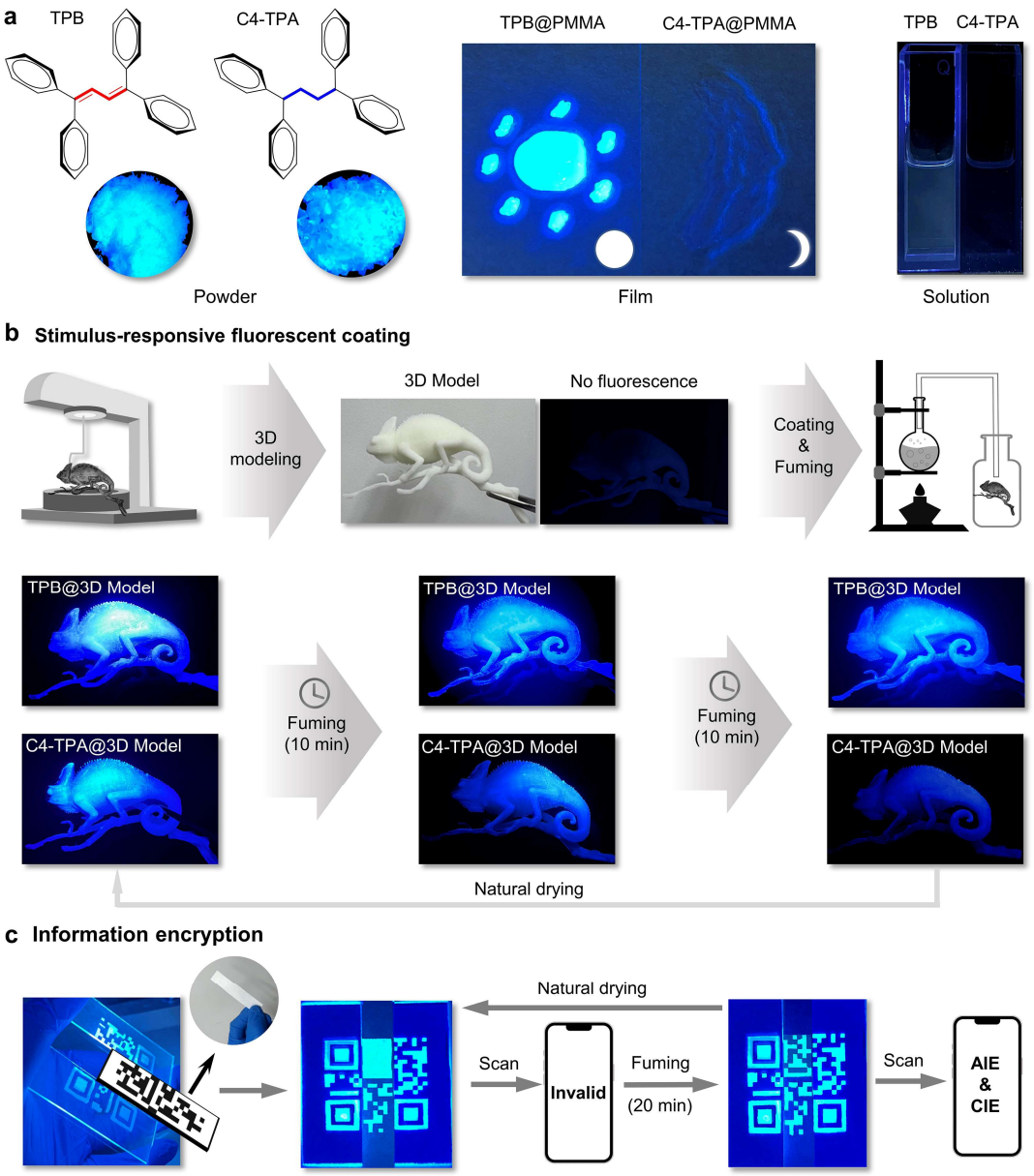

Fig. 6 | Stimulus-responsive nonconjugated luminogens. a Fluorescent photos of TPB and **C4-TPA** solids, the dispersed PMMA film (3 mg@60 mg PMMA), and the ACN solution (5×10^{-3} M) under λ_{ex} of 360 nm; **b** Time-dependent stimulus-responsive process of 3D models (chameleon) coated with conjugated TPB and nonconjugated **C4-TPA**, respectively. **c** Fluorescent encryption using the combination of TPB, and **C4-TPA**.